An improved smaller biotin ligase for BioID proximity labeling

Dae In Kim[a], Samuel C. Jensen[a], Kyle A. Noble[b], Birendra KC[a], Kenneth H. Roux[b], Khatereh Motamedchaboki[c], and Kyle J. Roux[a,d,*]

[a]Sanford Children's Health Research Center, Sanford Research, Sioux Falls, SD 57104; [b]Department of Biological Science, Florida State University, Tallahassee, FL 32306; [c]Sanford-Burnham Proteomics Facility, Sanford-Burnham Medical Research Institute, La Jolla, CA 92037; [d]Department of Pediatrics, Sanford School of Medicine, University of South Dakota, Sioux Falls, SD 57105

ABSTRACT **The BioID method uses a promiscuous biotin ligase to detect protein–protein associations as well as proximate proteins in living cells. Here we report improvements to the BioID method centered on BioID2, a substantially smaller promiscuous biotin ligase. BioID2 enables more-selective targeting of fusion proteins, requires less biotin supplementation, and exhibits enhanced labeling of proximate proteins. Thus BioID2 improves the efficiency of screening for protein–protein associations. We also demonstrate that the biotinylation range of BioID2 can be considerably modulated using flexible linkers, thus enabling application-specific adjustment of the biotin-labeling radius.**

Monitoring Editor
Yixian Zheng
Carnegie Institution

Received: Dec 18, 2015
Revised: Feb 4, 2016
Accepted: Feb 16, 2016

INTRODUCTION

Identification of protein–protein associations (PPAs) is a fundamental approach to the study of protein function, subcellular proteomes, and biological mechanisms. The proximity-dependent biotin identification (BioID) method was developed to overcome barriers imposed by conventional screening methods for PPAs (Roux *et al.*, 2012). The BioID method is based on proximity-dependent cellular biotinylation by a promiscuous bacterial biotin ligase (*Escherichia coli* BirA R118G, hereafter called BioID; Choi-Rhee *et al.*, 2004; Cronan, 2005) fused to a bait protein to generate a history of PPAs over time in living cells (Roux *et al.*, 2012). These biotinylated proteins can be selectively isolated by conventional biotin capture methods and identified using mass spectrometry (MS) analysis (Roux *et al.*, 2012, 2013; Kim *et al.*, 2014; Mehus *et al.*, 2016). These candidates identified by the BioID method can represent direct interactors, indirect interactors, and/or vicinal proteins that do not physically interact with the fusion protein.

Owing to its applicability to insoluble proteins and weak/transient PPAs, the BioID method has rapidly become widely used to study PPAs in the nuclear envelope (Roux *et al.*, 2012; Kim *et al.*, 2014), centrosomes (Comartin *et al.*, 2013; Firat-Karalar *et al.*, 2014), cell–cell junctions (Van Itallie *et al.*, 2013, 2014; Guo *et al.*, 2014; Steed *et al.*, 2014; Ueda *et al.*, 2015), spatiotemporal dynamics of epigenetic factors (Lambert *et al.*, 2015; Mulholland *et al.*, 2015), cancer development (Elzi *et al.*, 2014; Cole *et al.*, 2015; Dingar *et al.*, 2015), cross-talk between cytoskeletons (Jiu *et al.*, 2015), mRNA decay (Nishimura *et al.*, 2015), signaling pathways regulating various essential cellular mechanisms (Couzens *et al.*, 2013; Cheng *et al.*, 2015; Rodriguez-Fraticelli *et al.*, 2015; Schumacher *et al.*, 2015; Zhou *et al.*, 2015), and ubiquitin metabolism (Coyaud *et al.*, 2015; Yeh *et al.*, 2015). BioID has also been applied to elucidate interplay mechanisms between host and virus or microorganisms for HIV (Kueck *et al.*, 2015; Le Sage *et al.*, 2015; Ritchie *et al.*, 2015), *Chlamydia trachomatis* (Kabeiseman *et al.*, 2014), *Chlamydia psittaci* (Mojica *et al.*, 2015), *Toxoplasma gondii* (Chen *et al.*, 2015), *Trypanosoma brucei* (Morriswood *et al.*, 2013; McAllaster *et al.*, 2015), and herpes viruses (Lajko *et al.*, 2015)

One challenge for any method that relies on expression of fusion proteins is proper subcellular targeting. Although BioID (321 amino acids) is slightly larger than green fluorescent protein, we have observed that fusion to BioID occasionally prevents efficient targeting of certain fusion proteins. In attempt to ameliorate that limitation, we report our development and analysis of a new, smaller promiscuous

This article was published online ahead of print in MBoC in Press (http://www.molbiolcell.org/cgi/doi/10.1091/mbc.E15-12-0844) on February 24, 2016.

*Address correspondence to: Kyle J. Roux (kyle.roux@sanfordhealth.org).

Abbreviations used: BioID, proximity-dependent biotin identification; LaA, lamin A; NPC, nuclear pore complex; PPA, protein-protein association.

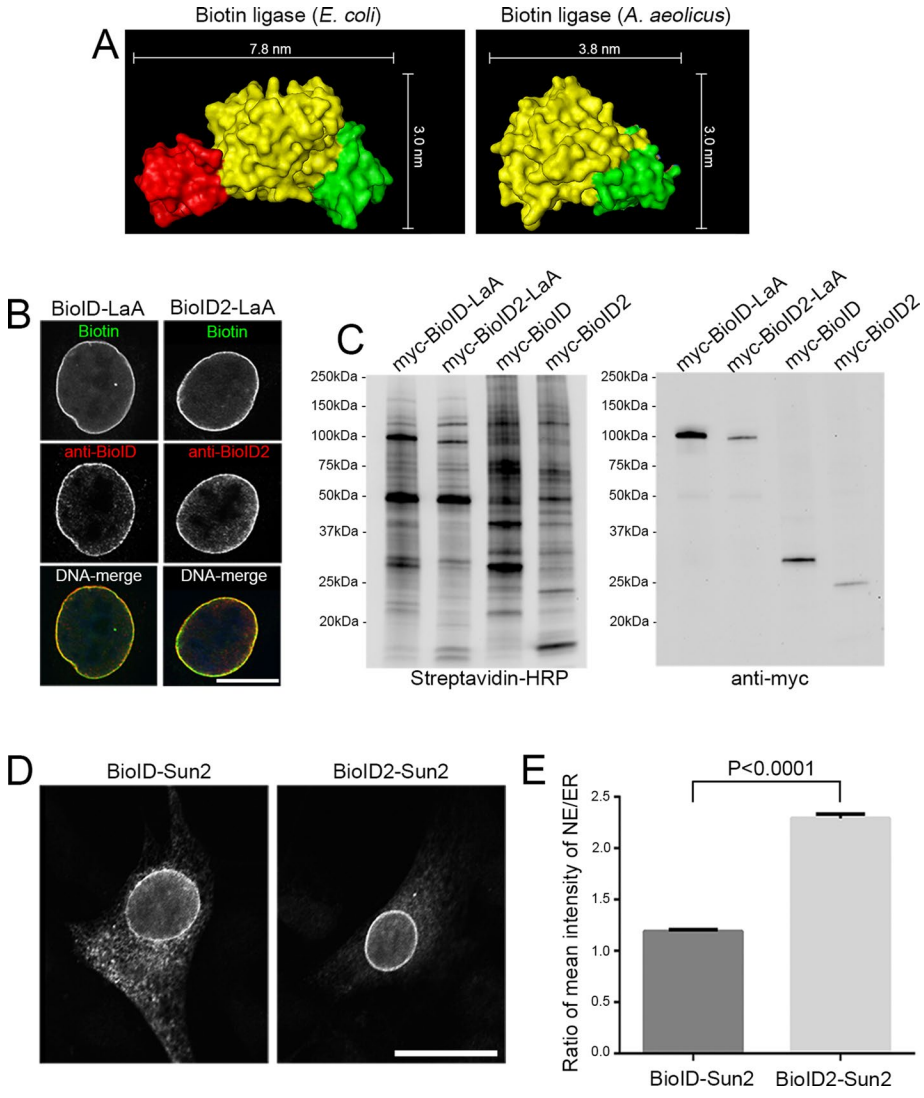

FIGURE 1: Promiscuous biotinylation by BioID2. (A) The dimensions of *E. coli* (left; PDB ID 1BIA) and *A. aeolicus* (right; PDB ID 2EAY) biotin ligases based on prior structural analyses. The catalytic (yellow), ATP-binding (green), and DNA-binding (red) domains. (B) BioID and BioID2 were fused with LaA and expressed in HEK293 cells. Fusion proteins were detected by specific antibodies against BioID or BioID2, respectively (red). Biotinylated proteins were labeled with streptavidin (green). DNA was labeled with Hoechst dye 33258 (blue). Scale bar, 10 μm. (C) Proteins biotinylated by BioID-LaA, BioID2-LaA, BioID-only, or BioID2-only were detected with HRP-conjugated streptavidin after SDS–PAGE separation. Expression of either promiscuous ligase leads to biotinylation of endogenous proteins (left). Fusion proteins were detected with anti-myc antibodies (right). (D) BioID-human Sun2 or BioID2-human Sun2 were transiently expressed in NIH3T3 cells. Fusion proteins were detected using an anti-Sun2 antibody incapable of detecting murine Sun2. Scale bar, 10 μm. (E) The NE/ER ratio of the mean intensity of BioID-human Sun2 or BioID2-human Sun2 detected with anti-human Sun2. Values are mean ± SEM. We measured 48 nuclei/condition.

biotin ligase that, in addition to its smaller size, is more efficient at labeling proximate proteins.

RESULTS AND DISCUSSION

A smaller promiscuous biotin ligase, BioID2, improves localization of its fusion protein

We first attempted to reduce the size of BioID through targeted deletion of the N-terminal DNA-binding domain of the enzyme; however, the resultant products failed to retain enzymatic activity (unpublished data) as expected from subsequent studies showing that this region is critical for BirA biotin ligase activity (Henke and Cronan, 2014). With our second approach, we used Uniprot to identify the smallest known biotin ligase, which is from *Aquifex aeolicus*. Based on the published protein crystallography, biotin ligases from *A. aeolicus* and *E. coli* share similarities in their overall structures (Wilson *et al.*, 1992; Tron *et al.*, 2009). However, the biotin ligase from *A. aeolicus* (233 amino acids) lacks the DNA-binding domain and is substantially smaller (Figure 1A). To create a smaller enzyme for proximity-dependent biotinylation, we humanized the biotin ligase of *A. aeolicus* and mutated a conserved residue within the biotin catalytic domain (R40G) in an attempt to enable promiscuous biotinylation (Choi-Rhee *et al.*, 2004; Cronan, 2005). Called BioID2, this smaller ligase was tested for promiscuous biotinylation in live mammalian cells. BioID and BioID2 were each fused to the highly insoluble nuclear protein lamin A (LaA) and expressed in HEK293 cells. Both fusion proteins were predominantly localized at the nuclear envelope (NE), leading to biotinylation of proteins at the NE (Figure 1, B and C). Thus the BioID2 appears at least fundamentally comparable to the original BioID in living mammalian cells. Because BioID2 is substantially smaller than BioID, we tested whether BioID2 improves localization of its fusion protein other than LaA. To this end, we transiently expressed human Sun2 with N-terminal BioID or BioID2 in a mouse fibroblast NIH3T3. Sun2 is a type II NE protein with an N-terminal nucleoplasmic domain. Like many other NE proteins, Sun2 is sensitive to endoplasmic reticulum mislocalization upon the fusion of bulky motifs to its N-terminus (Antonin *et al.*, 2011; Ungricht *et al.*, 2015). Compared with BioID, BioID2 enabled a more appropriate targeting of Sun2 to the NE when the proteins were expressed at comparable levels (Figure 1D). The relative mean intensity of the expressed Sun2 at the NE compared with the endoplasmic reticulum (ER) indicates that BioID2-Sun2 is approximately twofold more concentrated at the NE than BioID-Sun2 (Figure 1E). These results support the conventional wisdom that a smaller tag is less disruptive to a fusion protein. In addition, because *A. aeolicus* is a thermophilic bacterium, we predicted that the BioID2 might optimally function at higher temperatures. To monitor the influence of temperature on promiscuous biotinylation by BioID and BioID2, we performed in vitro biotinylation assays using bovine serum albumin (BSA) as substrate. Among the tested temperatures, biotinylation by BioID2 was optimal at 50°C, whereas biotinylation by BioID was optimal at 37°C. Both enzymes exhibited reduced activity below 37°C (Supplemental Figure S1). These observations suggest that BioID2 would be the preferred ligase for thermophilic

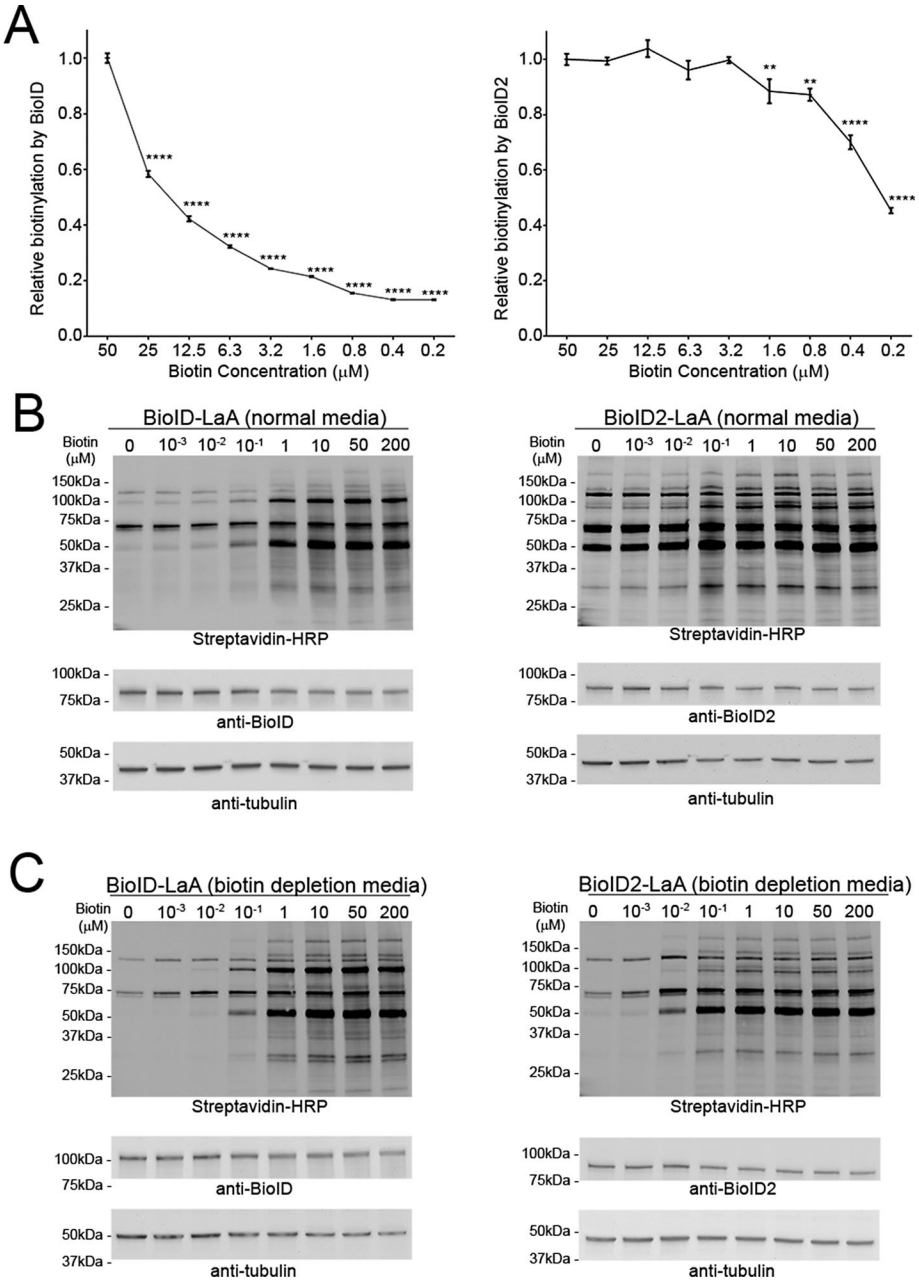

FIGURE 2: BioID2 requires less biotin than does BioID for promiscuous biotinylation. (A) In vitro biotinylation at variable biotin concentrations was performed using purified BioID (left) and BioID2 (right). Values are mean ±SEM. ****$p < 0.0001$ and **$p < 0.01$ as compared with the 50 μM concentration. Each group consisted of three replicates. (B) Cellular biotinylation at variable biotin concentrations was analyzed using cells stably expressing BioID-LaA (left) and BioID2-LaA (right) in culture media supplemented with 10% fetal bovine serum. Biotinylation was measured after incubation with the indicated concentration of biotin for 16 h. (C) Cellular biotinylation at variable biotin concentration was analyzed using cells stably expressing BioID-LaA (left) and BioID2-LaA (right). Biotin-depleted medium was used to inhibit basal biotinylation. Biotinylation by BioID-LaA or BioID2-LaA was analyzed after incubation with the indicated concentration of biotin for 16 h.

conditions but is also highly efficient at biotinylating proximate proteins in live cells at 37°C.

BioID2 requires less biotin than BioID

We next used purified BioID and BioID2 to compare their requirements for biotin supplementation. BioID or BioID2 were incubated with BSA for 16 h with 0.2–50 μM biotin. Biotinylation by BioID was markedly reduced as the concentration of biotin decreased below 50 μM, whereas BioID2 sustained maximum biotinylation through 3.2 μM biotin (Figure 2A). Similar results were observed in HEK293 cells stably expressing BioID-LaA or BioID2-LaA and incubated for 16 h with 0.001–200 μM biotin. BioID2-LaA exhibited saturation of biotinylation at 0.1 μM biotin; however, biotinylation by BioID-LaA required 1 μM biotin for maximum biotinylation. Of interest, we noted some basal biotinylation in the BioID2-LaA cells under conditions with no biotin supplementation (Figure 2B). The basal biotinylation is likely induced by BioID2-LaA responding to the low levels of biotin in serum included with the culture medium since it was inhibited by culturing cells for 72 h in medium with biotin-depleted serum. To rule out accumulation of basal biotinylation in normal medium, we monitored biotinylation by BioID2-LaA under biotin-depleted conditions. Under these conditions, BioID2-LaA generated detectable biotinylation from 0.01 μM biotin, whereas BioID-LaA required 0.1 μM biotin (Figure 2C). However, biotinylation by both BioID-LaA and BioID2-LaA reached maximal levels ~16 h after addition of biotin under conditions of biotin saturation (50 μM; Supplemental Figure S2). This observation suggests that biotin depletion conditions might need to be used for time-sensitive studies using BioID2 (e.g., comparing drug-treated to control conditions) to more exclusively capture protein associations that occur during a discrete time frame. However, the higher efficacy of BioID2 with lower biotin concentrations would be a useful characteristic when performing BioID in model systems such as *Caenorhabditis elegans*, *Drosophila melanogaster*, or *Mus musculus* in which biotin supplementation might be more complicated than simple medium supplementation.

BioID and BioID2 are functionally comparable

To compare the practical efficacy of BioID2 to that of original BioID, we evaluated candidates identified by both enzymes when targeted to a highly stable and structurally well-characterized protein complex. To this end, we C-terminally fused BioID and BioID2 to Nup43, a constituent of the highly stable Nup107–Nup160 complex that serves as a structural subcomplex of the nuclear pore complex (NPC; Daigle *et al.*, 2001; Loiodice *et al.*, 2004; D'Angelo *et al.*, 2009; Savas *et al.*, 2012). When stably expressed in HEK293 cells, Nup43-BioID and Nup43-BioID2 both target to the NPC (Supplemental Figure S3) and biotinylate endogenous proteins localized at the NPC when supplemented with

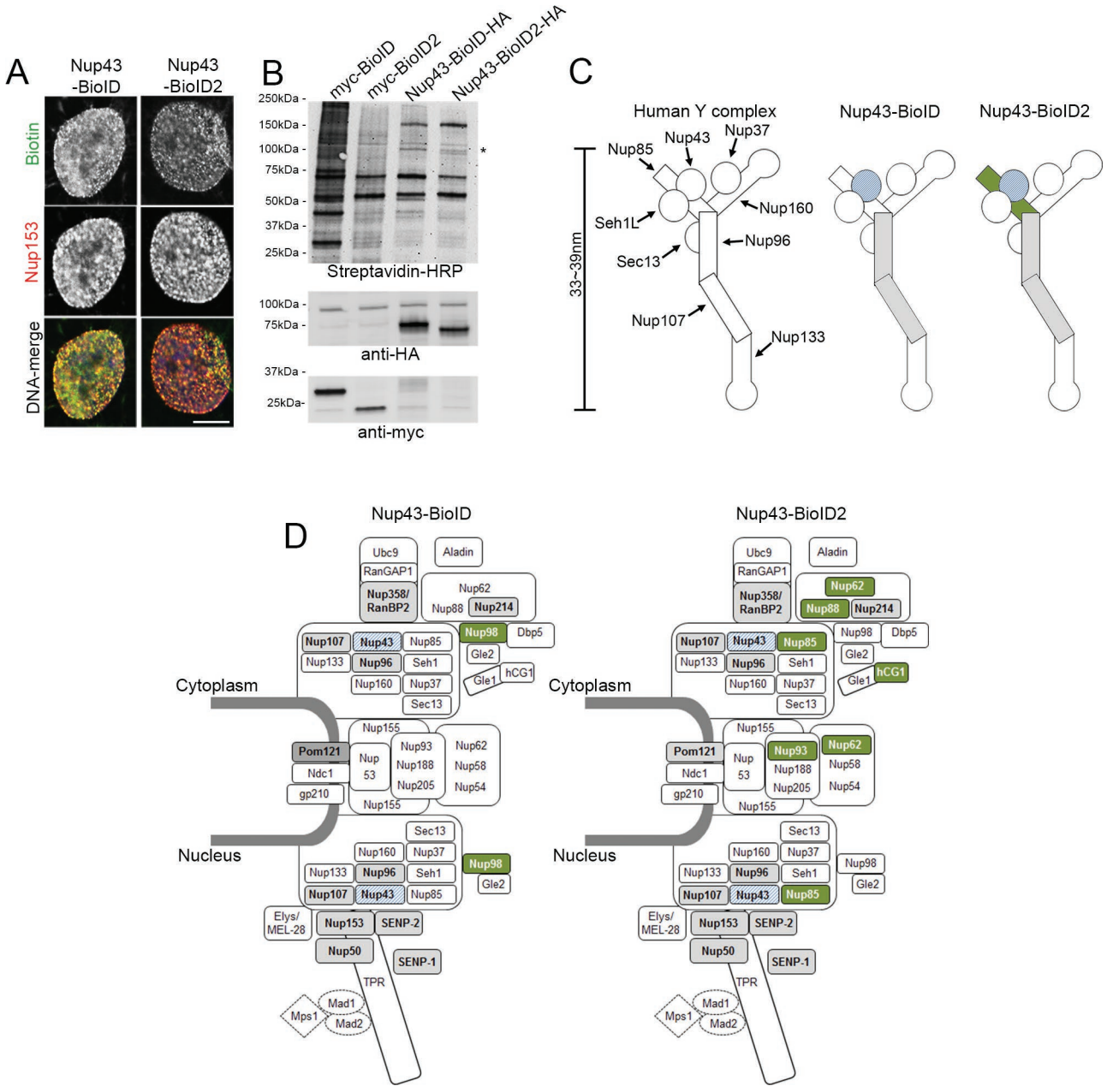

FIGURE 3: Application of BioID2 to the human Nup107–Nup160 complex. (A) Expression of Nup43-BioID or Nup43-BioID2 biotinylated endogenous proteins at the NPC. The NPCs were labeled with an anti-Nup153 antibody (red). Biotinylated proteins were detected with streptavidin (green). DNA was labeled with Hoechst dye 33258 (blue). To observe more clearly the NPCs, confocal images were taken at the surface of the NE. Scale bar, 10 μm. (B) Proteins biotinylated by Nup43-BioID and Nup43-BioID2 were detected with HRP-conjugated streptavidin (top). Fusion proteins were detected with anti-HA antibody (middle). BioID- or BioID2-only controls were detected by an anti-myc antibody (bottom). Asterisk indicates predicted migration of Nup96 and Nup107. (C) Model of the Nup107–Nup160 complex based on the previous literature and resolved structures (Hoelz *et al.*, 2011; Bui *et al.*, 2013). Candidates identified by both Nup43-BioID (middle) and Nup43-BioID2 (right) are labeled gray. Uniquely detected candidates are colored in green, and fusion proteins are indicated with blue. Modified from Kim *et al.* (2014). (D) The full range of NPC candidates, with those identified by both Nup43-BioID (left) and Nup43-BioID2 (right) labeled gray. Uniquely detected candidates are colored in green, and fusion proteins are indicated with patterned blue. Modified from Kim *et al.* (2014).

50 μM biotin (Figure 3, A and B). To reveal the identity of these endogenous proteins, we followed large-scale pull downs of biotinylated proteins by MS analysis. These results revealed that ~40% of spectral counts detected by Nup43-BioID are NPC-associated proteins (Nups), whereas ~60% of spectral counts detected by Nup43-BioID2 are Nups (Supplemental Table S1). Of note, the vast majority of abundant candidates that account for ~90% of total spectra counts are commonly detected by Nup43-BioID or Nup43-BioID2 (Supplemental Table S1). Similarly, 60% of detected background proteins are commonly identified from BioID-only and BioID2-only. Those commonly identified proteins are clearly abundant proteins since they account for ~87% of total spectra counts (Supplemental Table S3).

In all, this comparative BioID analysis at the NPC demonstrates the specificity and functionality of BioID2 in screening for PPAs.

Within the Nup107–Nup160 complex, both Nup43-BioID and Nup43-BioID2 detected Nup96 and Nup107 (Figure 3C). Nup85, a direct interacting protein of Nup43, is not efficiently biotinylated by Nup43-BioID (Kim *et al.*, 2014). However, Nup43-BioID2 was able to detect Nup85 (Figure 3C), suggesting that BioID2 might be more efficient at biotinylating proximate proteins. We also put a 5-nm linker consisting of three repeats of GGGGS between Nup43 and BioID to resolve any steric hindrance that potentially inhibits biotinylation of Nup85 by Nup43-BioID. However, Nup85 was not detected by Nup43-BIoID with the 5-nm linker (unpublished data). Thus these observations suggest that BioID2 may be more efficient in biotinylation. When examining the Nups outside of the Nup107–Nup160 complex that were detected by Nup43-BioID and Nup43-BioID2, we observed that Nups located proximate to the Nup107–Nup160 complex were commonly detected (Figure 3D). For instance, the proximate location between the Y-complex and nuclear basket Nups such as Nup153 has been documented by biochemical experiments, cross-linking-MS (XL-MS), and cryo–electron tomography (cryo-ET) studies (Vasu *et al.*, 2001; Bui *et al.*, 2013). In addition, the flexibility of nuclear basket proteins may also enable contact with Nup43 (Fahrenkrog *et al.*, 2002). Nup43-BioID2 also detected hCG1, a cytoplasmic Nup associated with Nup214 through the direct interaction with Gle1 (Kendirgi *et al.*, 2005; Folkmann *et al.*, 2013), and central NPC constituents such as Nup62 and Nup93 (Figure 3D). This detection of distally located Nups by Nup43-BioID2 also suggests that the practical biotinylation range of BioID2 might be somewhat larger than that of BioID and/or that BioID2 is capable of detecting proteins refractory to detection by the original BioID.

The biotinylation range can be increased with a flexible linker

The practical labeling radius of promiscuous biotin ligases is an important experimental consideration since a large radius would predictably detect more proteins that may not be direct interactors of the bait, whereas, conversely, a smaller radius would potentially limit detection of relevant protein interactors for a larger protein or a protein complex. Our previous studies indicated the practical labeling radius of BioID is ~10 nm (Kim *et al.*, 2014). We hypothesized that the biotinylation range of BioID2 could be increased using a flexible linker. To test this hypothesis, we inserted a 25-nm linker consisting of 13 repeats of GGGGS (Amet *et al.*, 2009) between Nup43 and BioID2 (Nup43-Linker-BioID2; Figure 4A). In HEK293 cells stably expressing Nup43-Linker-BioID2, the fusion protein was localized at the NPC (Supplemental Figure S3) and biotinylated proteins at the NPC (Figure 4C). The insertion of the linker did not lead to any abnormal proteolytic processing of the fusion protein and enabled biotinylation of endogenous proteins in live cells (Figure 4B). Given the size of the Nup107–Nup160 complex, Nup43-Linker-BioID2 can theoretically access all the constituents of the complex. Indeed, by MS analysis of a large-scale BioID pull down, Nup43-Linker-BioID2 detected all the constituents of the Nup107–Nup160 complex, including distal tip Nups such as Nup160 and Nup133 (Figure 4D). Outside the Nup107–Nup160 complex, central channel proteins Nup205 and Nup62 were also uniquely detected by the addition of the linker (Figure 4E). Of interest, in Nup43-Linker-BioID2, karyopherins that mediate transport across the NPC were also detected, presumably because the linker allows the ligase to occasionally contact the karyopherins in the central channel (Supplemental Table S2). Our data suggest that the biotinylation range of BioID2 can be increased using a molecular linker, thus enabling identification of proteins well beyond the range of the ligase alone. However, despite the detection of substantially more NPC proteins than Nup43-BioID2, Nup43-Linker-BioID2 did not dramatically increase the detection of candidates outside of the Nup107–Nup160 complex. This observation might indicate the preserved specificity to the region proximate to Nup43.

In summary, BioID2 is fundamentally comparable to BioID in its ability to promiscuously biotinylate proximate proteins but requires considerably less biotin, which may facilitate application of the BioID method to model systems for which biotin supplementation methods are limited. With its smaller size, BioID2 should enable a more appropriate targeting and thus function of fusion proteins. In addition, the biotinylation range and/or efficacy of BioID2 appear enhanced compared with those of BioID, thus enabling detection of proteins that are refractory to biotinylation with the original ligase. In addition, we demonstrated that the use of flexible linkers can increase the labeling radius of BioID2, thereby overcoming limitations inherent to the intrinsic biotinylation range of BioID ligases. This will provide users of the BioID method flexibility in experimental design when studying larger proteins whose spatial dimensions exceed the biotinylation range, probing the constituency of large protein complexes, or globally surveying the protein constituency of discrete subcellular domains.

MATERIALS AND METHODS

Plasmids

Humanized BioID2 was synthesized and amplified by PCR. The amplified BioID2 was inserted into the previously generated BioID-LaA pcDNA 3.1 vector (Kim *et al.*, 2014) via *Nhe*I and *Xho*I to replace BioID with BioID2. BioID-LaA and BioID2-LaA in pcDNA 3.1 were amplified by PCR and inserted into pBabe.puro using *Eco*RI and *Sal*I. BioID2 was amplified by PCR and inserted into the previously generated Nup43-BioID pcDNA 3.1 vector (Kim *et al.*, 2014) using *Bam*HI and *Pme*I to replace BioID with BioID2. Nup43-BioID and Nup43-BioID2 in pcDNA 3.1 were subcloned to pBabe.puro using *Eco*RI and *Sal*I. Linker-BioID was synthesized and amplified by PCR. The PCR products were inserted into the Nup43-BioID pcDNA 3.1 vector (Kim *et al.*, 2014) via *Eco*RI and *Pme*I to replace BioID with Linker-BioID. BioID2 was amplified and inserted to Nup43-Linker-BioID using *Bam*HI and *Pme*I to replace BioID with BioID2. Nup43-Linker-BioID and Nup43-Linker-BioID2 in pcDNA 3.1 vector were subcloned to pBabe.puro using *Eco*RI and *Sal*I. To generate HA-BioID-LaA and HA-BioID2-LaA, BioID and BioID2 were amplified with primers containing sequences for HA. The PCR products were inserted into the previously generated BioID-LaA pcDNA 3.1 vector using *Nhe*I and *Xho*1. To generate glutathione *S*-transferase (GST) fusion protein, BioID and BioID2 were amplified by PCR and inserted into pGex 4T-1 vector (GE Healthcare Life Sciences, Pittsburgh, PA) using *Eco*RI and *Xho*I.

Structural analysis

Previously published Protein Data Bank (PDB) structures of the biotin ligase from *E. coli* (DOI 10.2210/pdb1bia/pdb) (Wilson *et al.*, 1992) and *A. aeolicus* (DOI 10.2210/pdb2eay/pdb) were analyzed by MacPyMOL (www.pymol.com).

Immunofluorescence

Stable cells were fixed in 3% (wt/vol) paraformaldehyde/phosphate-buffered saline (PBS) for 10 min. Cells were permeabilized by 0.4% (wt/vol) Triton X-100/PBS for 15 min, followed by 0.5% SDS/PBS for 5 min. Cells were labeled with the following primary antibodies: chicken polyclonal anti-BirA (1:2000, ab14002; Abcam, Cambridge, MA), rabbit polyclonal anti-myc (1:1000, ab9106; Abcam), rabbit polyclonal anti-hemagglutinin (HA; 1:1000, ab9110; Abcam), and

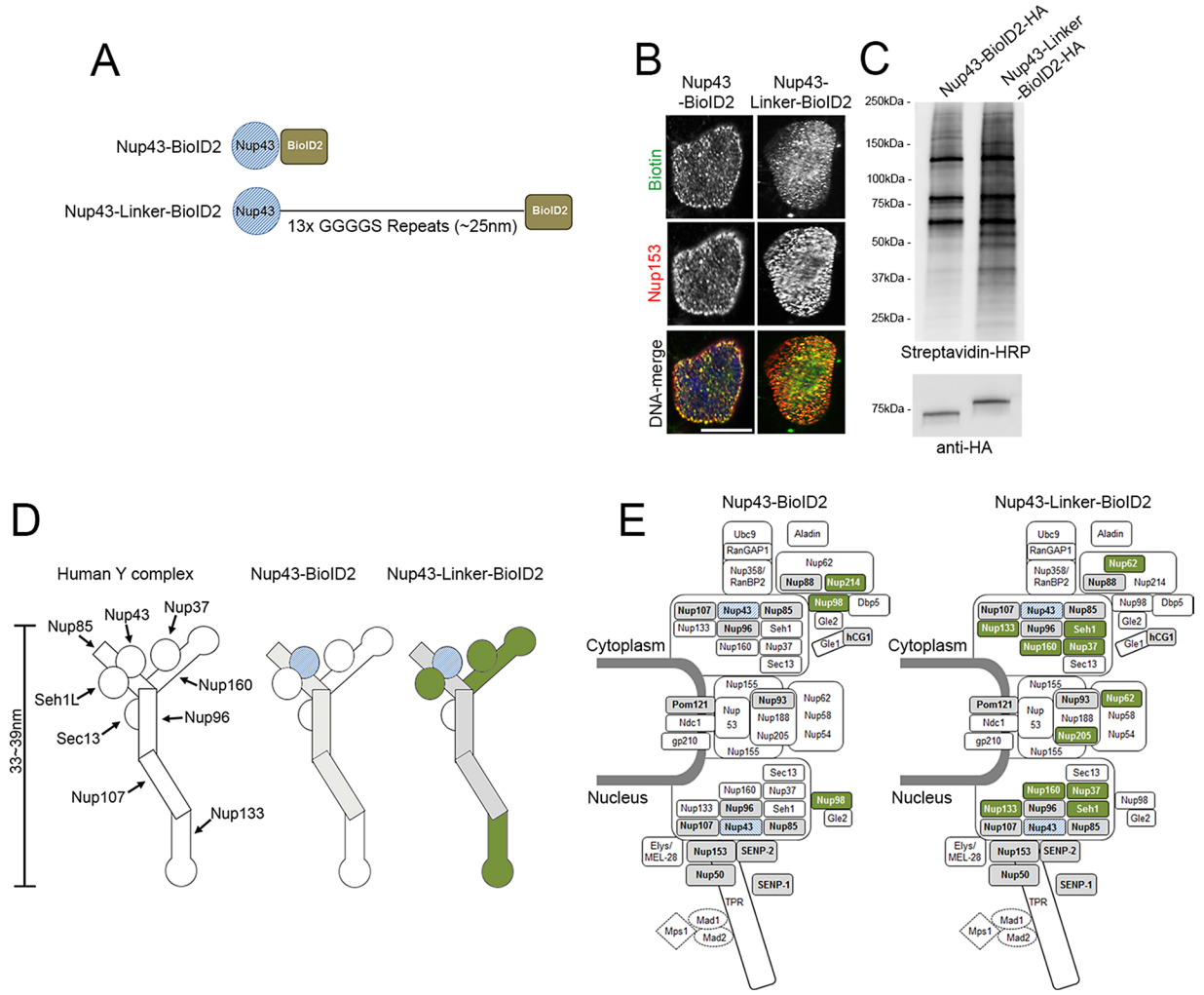

FIGURE 4: An extended flexible linker increases the number of candidates detected by Nup43-BioID2. (A) Linear model of Nup43-BioID2 and Nup43-Linker-BioID2 fusion proteins. An extended flexible linker consisting of 13 repeats of GGGGS predicted to provide an ~25-nm extension was inserted between the Nup43 bait and BioID2 ligase. (B) Expression of Nup43-BioID2 or Nup43-Linker-BioID2 led to biotinylation of endogenous proteins at the NPC. NPCs were labeled using an anti-Nup153 antibody (red). Biotinylated proteins were detected with streptavidin (green). DNA was labeled with Hoechst dye 33258 (blue). Images were taken at the surface of the NE by confocal microscopy. Scale bar, 10 μm. (C) Proteins biotinylated by Nup43-BioID2 and Nup43-Linker-BioID2 were detected with HRP-conjugated streptavidin (top). Fusion proteins were labeled with anti-HA antibody (bottom). (D) Nup107–Nup160 complex candidates identified by both Nup43-BioID2 (middle) and Nup43-Linker-BioID2 (right) are labeled gray. Uniquely detected candidates are colored in green, and fusion proteins are indicated with blue. (E) For the entire NPC, Nups identified by both Nup43-BioID2 (left) and Nup43-Linker-BioID2 (right) are labeled gray. Uniquely detected candidates are colored in green, and fusion proteins are indicated with patterned blue.

mouse monoclonal anti-Nup153 (SA1; Kim *et al.*, 2014). Owing to the difficulty in detecting the N-terminal myc tag by immunofluorescence (Supplemental Figure S4), we generated a chicken anti-BioID2 using purified GST-BioID2 (1:2000; Aves Labs, Tigard, OR). Primary antibodies were detected using Alexa Fluor 568–conjugated goat anti-chicken (1:1000, A11041; Life Technologies, Carlsbad, CA), goat anti-rabbit (1:1000, A11036; Life Technologies), and goat anti-mouse (1:1000, A11031; Life Technologies). Alexa Fluor 488–conjugated streptavidin (S32354; Life Technologies) was used to detect biotinylated proteins. DNA was detected with Hoechst dye 33258. Coverslips were mounted using 10% (wt/vol) Mowiol 4-88 (Polysciences, Warrington, PA). Images were obtained using a Nikon A1-confocal microscope (60×/1.49 oil APO TIRF Nikon objective) with a charge-coupled device camera (CoolSnap HQ; Photometrics) linked to a workstation running NES-Elements software (Nikon, Melville, NY).

After transient expression of BioID-Sun2 and BioID2-Sun2 in mouse NIH3T3 cells, the fusion proteins were detected using an anti–human Sun2 antibody (1:200, A001209; Sigma-Aldrich, St. Louis, MO) that does not detect murine Sun2. Images were taken using Nikon A1-confocal microscope. The mean intensity of the fusion proteins at the NE or ER was obtained using ImageJ software (National Institutes of Health, Bethesda, MD).

Immunoblot

To analyze total cell lysates using immunoblot, 1.2×10^6 cells were lysed in SDS–PAGE sample buffer, boiled for 5 min, and sonicated to shear DNA. Proteins were separated on 4–20% gradient gels (Mini-PROTEAN TGX; Bio-Rad, Hercules, CA) and transferred to nitrocellulose membrane (Bio-Rad). After blocking with 1% (wt/vol) BSA and 0.2% Triton X-100 in PBS for 10 min, membranes were

incubated with horseradish peroxidase (HRP)–conjugated streptavidin (1:40,000, ab7403; Abcam) for 40 min. The signals from antibodies were detected using enhanced chemiluminescence. After detecting biotinylated proteins, membranes were subjected to 1% (wt/vol) sodium azide and 1.5% (vol/vol) hydrogen peroxide for 10 min to quench the HRP activity from the previous analysis. After blocking with 10% (vol/vol) adult bovine serum and 0.2% Triton X-100 in PBS for 20 min, appropriate primary antibodies were added, including mouse monoclonal anti-tubulin (1:2000, T9026; Sigma-Aldrich). The primary antibodies were detected using HRP-conjugated anti-chicken (1:40,000, A9046; Sigma-Aldrich), anti-rabbit (1:40,000, G21234; Life Technologies), or anti-mouse (1:40,000, F21453; Life Technologies) antibodies.

Cell culture

HEK293 cells were obtained from the American Type Culture Collection, Manassas, VA (ATCC CRL-1573), but not tested for contamination. Stable cell lines were generated using retroviral transduction. BioID and BioID2 in pBabe.puro vector were transfected into HEK293 Phoenix cells (National Gene Vector Biorepository, Indianapolis, IN) using Lipofectamine 2000 (Life Technologies) as recommended by the manufacturer. After overnight incubation at 37°C, the transfected cells were further incubated at 32°C for 36 h. The culture media were collected and centrifuged at 1000 × *g* for 5 min. The supernatant of the centrifuged media and Polybrene (4 μg/ml; Santa Cruz Biotechnology, Dallas, TX) were added to HEK293 cells. Puromycin (0.5 μg/ml; Fisher Scientific, Waltham, MA) was added to HEK293 cells 48 h after transduction. The expression of fusion proteins was further verified using immunofluorescence and immunoblotting. The stable cell lines were maintained in 5.0% CO_2 at 37°C in DMEM (HyClone, Logan, UT) supplemented with 10% fetal bovine serum (FBS). To prepare biotin-depleted media, 50 ml of DMEM supplemented with 10% FBS was incubated with 1 ml of Dynabeads (MyOne Streptavidin C1; Life Technologies) overnight and filtered with a 0.22-μm filter. Cells were incubated with biotin-depleted media for 72 h before analysis. Cell growth under the biotin-depleted media was carefully monitored. Because the members of the Nup107–Nup160 complex are associated with mitotic proteins (Zuccolo *et al*., 2007; Chatel and Fahrenkrog, 2011), large-scale BioID analyses for Nup43-BioID2 or Nup43-BioID were performed under growth-arresting low-serum conditions (DMEM supplemented with 0.1% FBS) to inhibit cell division.

Production of GST-fusion proteins

Expression of GST-fused BioID and BioID2 was induced with 1 mM isopropyl-β-D-thiogalactoside for 4 h at 37°C in a shaking incubator. The cell culture was then harvested by centrifugation at 6000 × *g* for 10 min. Harvested cells were resuspended in PBS and lysed with gentle sonication. Clarified lysate was incubated with glutathione resin (GBiosciences, St. Louis, MO) for 1 h with rotation and washed with five column volumes of PBS. Fusion proteins were eluted with three column volumes of 10 mM glutathione and 50 mM Tris, pH 8.0. Eluted fractions were then dialyzed against 1 l of PBS overnight. Protein concentration was measured based on ultraviolet absorbance at 280 nm.

In vitro assay

In vitro biotinylation reactions were performed in 500 nM BioID-GST or BioID fusion protein, 1.5 mM ATP, 1 mg/ml BSA, 1.8 mM β-mercaptoethanol, and a varied amount of biotin (50–800 μM) in PBS. Reactions were prepared in 0.5 ml and carried out overnight at 37°C. To investigate biotinylation in variable temperature, BioID and BioID2 reactions were prepared as previously described. The reactions were supplemented with 800 μM biotin and incubated overnight. The 96-well PCR thermocyclers (Applied Biosystems, Foster City, CA) were programmed with a single stage to hold a specific temperature for the duration of the reaction. A sample volume containing 1 μg of BSA from each reaction was coated onto a 96-well polystyrene plate in 0.1 M citric acid and 0.2 M sodium phosphate, pH 5.0, for 1 h and blocked overnight in 5% nonfat dry milk. Plates were washed with PBS-T (PBS with 0.05% Tween-20) and developed with streptavidin-HRP (Invitrogen, Carlsbad, CA). Detection was determined by incubation with *O*-phenylenediamine substrate (Invitrogen) for 10 min and quenching with 2 M sulfuric acid before measurement of the absorbance at 495 nm in a SpectraMax M5 plate reader (Molecular Devices, Sunnyvale, CA).

BioID pull down

For large-scale BioID pull down, 4×10^7 cells were incubated with 50 μM biotin for 16 h. After two times of PBS wash, the cells were lysed in 2.4 ml of lysis buffer containing 50 mM Tris, pH 7.4, 500 mM NaCl, 0.4% SDS, 1 mM dithiothreitol, and 1× Complete protease inhibitor (Halt Phosphatase Inhibitor Cocktail; Life Technologies). After collecting cells, Triton X-100 was added to 2% final concentration. After two times of sonication each for 1 min at 30% duty cycle and an output level of 4 (Sonifer-250; Branson), an equal volume of 50 mM Tris, pH 7.4, was added and cleaned using centrifugation at 16,500 × *g* for 10 min. The supernatant was collected to a 15-ml conical tube and incubated with 300 μl of Dynabeads overnight. Beads were collected using a magnetic stand and washed with twice with 2% (wt/vol) SDS, once with wash buffer containing 0.1% deoxycholate, 1% Triton X-100, 500 mM NaCl, 1 mM EDTA, and 50 mM 4-(2-hydroxyethyl)-1-piperazineethanesulfonic acid, pH 7.5, once with wash buffer containing 250 mM LiCl, 0.5% NP-40, 0.5% deoxycholate, 1 mM EDTA, and 10 mM Tris, pH 8, and once with 50 mM Tris. Ten percent of the samples were saved for further analysis. The other 90% of samples were resuspended in 50 mM NH_4HCO_3 for MS analysis.

Mass spectrometry analysis and data analysis

Tryptic digestion of proteins isolated by BioID pull down was performed using an optimized method (Kim *et al*., 2014). Beads were resuspended in 50 μl of 8 M urea/50 mM ammonium bicarbonate and proteins and reduced by adding 2 μl of 0.5 M Tris(2-carboxyethyl)phosphine to 50 μl of beads–proteins suspension mix for 60 min at 30°C. The reaction was cooled to room temperature before alkylation with 4 μl of 0.5 M iodoacetamide at room temperature in the dark for 30 min. Sample volume was adjusted by adding 350 μl of 50 mM ammonium bicarbonate to dilute the 8 M urea to 1 M before trypsin digestion. MS-grade trypsin (Promega, Madison, WI) was added (1:20 ratio for beads, 5 μg of total trypsin for BioID samples) for overnight digestion at 30°C using an Eppendorf Thermomixer at 700 rpm. Digested peptides were isolated from the beads by centrifugation and magnetic separation, and peptide digests were transferred to a new tube and washed with 50 μl of 50 mM ammonium bicarbonate before pooling of digestions. Formic acid was added to the peptide solution (to 2%), followed by desalting by Microtrap (77720; Thermo Scientific, Waltham, MA), and then one-dimensional liquid chromatography (LC)–MS/MS analysis of 10% of total digests in duplicate runs was performed by on-line analysis of peptides by a high-resolution, high-accuracy LC-MS/MS system consisting of an EASY-nLC 1000 HPLC, Acclaim PepMap peptide trap, 25 cm × 2 μm Easy-Spray C18 column, Easy Spray Source, and Q Exactive Plus mass spectrometer (all from Thermo

Fisher Scientific). A 225-min gradient consisting of 5–16% B (100% acetonitrile) in 140 min, 16–28% in 70 min, 28–38% in 10 min, and 38–85% in 5 min was used to separate the peptides. The total LC time was 250 min. The Q Exactive Plus was set to scan precursors at 70,000 resolution, followed by data-dependent MS/MS at 17,500 resolution of the top 12 precursors.

The LC-MS/MS raw data of three technical replicates were combined and submitted to Sorcerer Enterprise, version 3.5 (Sage-N Research, Milpitas, CA) with SEQUEST algorithm as the search program for peptide/protein identification. SEQUEST was set up to search the target-decoy EBI.IPI.HUAMAN (version 3.73) protein database containing protein sequences, using trypsin for enzyme with an allowance of up to two missed cleavages, Semi Tryptic search, fixed modification of 57 Da for cysteine to account for carboxyamidomethylation, and precursor mass tolerance of 50 ppm. Differential search includes 16 Da for methionine oxidation and 226 on lysine for biotinylation. The search results were viewed, sorted, filtered, and statistically analyzed by using comprehensive proteomics data analysis software Peptide/Protein prophet, version 4.02 (ISB). The minimum transproteomic pipeline (TPP) probability score for proteins was set to 0.9 to assure very low error (much less than a false discovery rate of 2%) with reasonably good sensitivity. The differential spectral count analysis was done by QTools, an open-source in-house–developed tool for automated differential peptide/protein spectral count analysis (Brill *et al.*, 2009). Proteins with fewer than three spectral counts or common MS background proteins, including keratins, histones, and ribosomal proteins, were removed due to the lack of confidence. Any candidate identified by Nup43-BioID or Nup43BioID2 was excluded if the relative percentage of total spectral counts was threefold less than in the BioID- or BioID2-only, respectively.

Statistical analysis

For the in vitro biotinylation assays, the biotinylation results are represented as mean ± SEM. Differences between multiple groups were compared by one-way analysis of variance (ANOVA) followed by Dunnett post-hoc test multiple comparisons. To compare the targeting ability of BioID-Sun2 and BioID2-Sun2, the relative mean intensity of the fusion proteins was analyzed by an unpaired *t* test.

ACKNOWLEDGMENTS

These studies were supported by Grants RO1GM102203, RO1GM102486, and RO1EB014869 to K.J.R. from the National Institutes of Health. These studies were facilitated by the Imaging Core and Protein Biochemistry Core at Sanford Research, which are supported by Institutional Development Awards from the National Institute of General Medical Sciences and the National Institutes of Health under Grants P20GM103548 and P20GM103620.

REFERENCES

Amet N, Lee HF, Shen WC (2009). Insertion of the designed helical linker led to increased expression of tf-based fusion proteins. Pharm Res 26, 523–528.

Antonin W, Ungricht R, Kutay U (2011). Traversing the NPC along the pore membrane: targeting of membrane proteins to the INM. Nucleus 2, 87–91.

Brill LM, Motamedchaboki K, Wu S, Wolf DA (2009). Comprehensive proteomic analysis of Schizosaccharomyces pombe by two-dimensional HPLC-tandem mass spectrometry. Methods 48, 311–319.

Bui KH, von Appen A, DiGuilio AL, Ori A, Sparks L, Mackmull MT, Bock T, Hagen W, Andres-Pons A, Glavy JS, *et al.* (2013). Integrated structural analysis of the human nuclear pore complex scaffold. Cell 155, 1233–1243.

Chatel G, Fahrenkrog B (2011). Nucleoporins: leaving the nuclear pore complex for a successful mitosis. Cell Signal 23, 1555–1562.

Chen AL, Kim EW, Toh JY, Vashisht AA, Rashoff AQ, Van C, Huang AS, Moon AS, Bell HN, Bentolila LA, *et al.* (2015). Novel components of the Toxoplasma inner membrane complex revealed by BioID. mBio 6, e02357–02314.

Cheng YS, Seibert O, Kloting N, Dietrich A, Strassburger K, Fernandez-Veledo S, Vendrell JJ, Zorzano A, Bluher M, Herzig S, *et al.* (2015). PPP2R5C couples hepatic glucose and lipid homeostasis. PLoS Genet 11, e1005561.

Choi-Rhee E, Schulman H, Cronan JE (2004). Promiscuous protein biotinylation by Escherichia coli biotin protein ligase. Protein Sci 13, 3043–3050.

Cole A, Wang Z, Coyaud E, Voisin V, Gronda M, Jitkova Y, Mattson R, Hurren R, Babovic S, Maclean N, *et al.* (2015). Inhibition of the mitochondrial protease ClpP as a therapeutic strategy for human acute myeloid leukemia. Cancer Cell 27, 864–876.

Comartin D, Gupta GD, Fussner E, Coyaud E, Hasegan M, Archinti M, Cheung SW, Pinchev D, Lawo S, Raught B, *et al.* (2013). CEP120 and SPICE1 cooperate with CPAP in centriole elongation. Curr Biol 23, 1360–1366.

Couzens AL, Knight JD, Kean MJ, Teo G, Weiss A, Dunham WH, Lin ZY, Bagshaw RD, Sicheri F, Pawson T, *et al.* (2013). Protein interaction network of the mammalian Hippo pathway reveals mechanisms of kinase-phosphatase interactions. Sci Signal 6, rs15.

Coyaud E, Mis M, Laurent EM, Dunham WH, Couzens AL, Robitaille M, Gingras AC, Angers S, Raught B (2015). BioID-based identification of Skp Cullin F-box (SCF)beta-TrCP1/2 E3 ligase substrates. Mol Cell Proteomics 14, 1781–1795.

Cronan JE (2005). Targeted and proximity-dependent promiscuous protein biotinylation by a mutant Escherichia coli biotin protein ligase. J Nutr Biochem 16, 416–418.

Daigle N, Beaudouin J, Hartnell L, Imreh G, Hallberg E, Lippincott-Schwartz J, Ellenberg J (2001). Nuclear pore complexes form immobile networks and have a very low turnover in live mammalian cells. J Cell Biol 154, 71–84.

D'Angelo MA, Raices M, Panowski SH, Hetzer MW (2009). Age-dependent deterioration of nuclear pore complexes causes a loss of nuclear integrity in postmitotic cells. Cell 136, 284–295.

Dingar D, Kalkat M, Chan PK, Srikumar T, Bailey SD, Tu WB, Coyaud E, Ponzielli R, Kolyar M, Jurisica I, *et al.* (2015). BioID identifies novel c-MYC interacting partners in cultured cells and xenograft tumors. J Proteomics 118, 95–111.

Elzi DJ, Song M, Hakala K, Weintraub ST, Shiio Y (2014). Proteomic analysis of the EWS-Fli-1 interactome reveals the role of the lysosome in EWS-Fli-1 turnover. J Proteome Res 13, 3783–3791.

Fahrenkrog B, Maco B, Fager AM, Koser J, Sauder U, Ullman KS, Aebi U (2002). Domain-specific antibodies reveal multiple-site topology of Nup153 within the nuclear pore complex. J Struct Biol 140, 254–267.

Firat-Karalar EN, Rauniyar N, Yates JR 3rd, Stearns T (2014). Proximity interactions among centrosome components identify regulators of centriole duplication. Curr Biol 24, 664–670.

Folkmann AW, Collier SE, Zhan X, Aditi , Ohi MD, Wente SR (2013). Gle1 functions during mRNA export in an oligomeric complex that is altered in human disease. Cell 155, 582–593.

Guo Z, Neilson LJ, Zhong H, Murray PS, Zanivan S, Zaidel-Bar R (2014). E-cadherin interactome complexity and robustness resolved by quantitative proteomics. Sci Signal 7, rs7.

Henke SK, Cronan JE (2014). Successful conversion of the Bacillus subtilis BirA Group II biotin protein ligase into a Group I ligase. PLoS One 9, e96757.

Hoelz A, Debler EW, Blobel G (2011). The structure of the nuclear pore complex. Annu Rev Biochem 80, 613–643.

Jiu Y, Lehtimaki J, Tojkander S, Cheng F, Jaalinoja H, Liu X, Varjosalo M, Eriksson JE, Lappalainen P (2015). Bidirectional interplay between vimentin intermediate filaments and contractile actin stress fibers. Cell Rep 11, 1511–1518.

Kabeiseman EJ, Cichos KH, Moore ER (2014). The eukaryotic signal sequence, YGRL, targets the chlamydial inclusion. Front Cell Infect Microbiol 4, 129.

Kendirgi F, Rexer DJ, Alcazar-Roman AR, Onishko HM, Wente SR (2005). Interaction between the shuttling mRNA export factor Gle1 and the nucleoporin hCG1: a conserved mechanism in the export of Hsp70 mRNA. Mol Biol Cell 16, 4304–4315.

Kim DI, Birendra KC, Zhu W, Motamedchaboki K, Doye V, Roux KJ (2014). Probing nuclear pore complex architecture with proximity-dependent biotinylation. Proc Natl Acad Sci USA 111, E2453–E2461.

Kueck T, Foster TL, Weinelt J, Sumner JC, Pickering S, Neil SJ (2015). Serine phosphorylation of HIV-1 Vpu and its binding to tetherin regulates interaction with clathrin adaptors. PLoS Pathog 11, e1005141.

Lajko M, Haddad AF, Robinson CA, Connolly SA (2015). Using proximity biotinylation to detect herpesvirus entry glycoprotein interactions: limitations for integral membrane glycoproteins. J Virol Methods 221, 81–89.

Lambert JP, Tucholska M, Go C, Knight JD, Gingras AC (2015). Proximity biotinylation and affinity purification are complementary approaches for the interactome mapping of chromatin-associated protein complexes. J Proteomics 118, 81–94.

Le Sage V, Cinti A, Valiente-Echeverria F, Mouland AJ (2015). Proteomic analysis of HIV-1 Gag interacting partners using proximity-dependent biotinylation. Virol J 12, 138.

Loiodice I, Alves A, Rabut G, Van Overbeek M, Ellenberg J, Sibarita JB, Doye V (2004). The entire Nup107-160 complex, including three new members, is targeted as one entity to kinetochores in mitosis. Mol Biol Cell 15, 3333–3344.

McAllaster MR, Ikeda KN, Lozano-Nunez A, Anrather D, Unterwurzacher V, Gossenreiter T, Perry JA, Crickley R, Mercadante CJ, Vaughan S, *et al.* (2015). Proteomic identification of novel cytoskeletal proteins associated with TbPLK, an essential regulator of cell morphogenesis in Trypanosoma brucei. Mol Biol Cell 26, 3013–3029.

Mehus AA, Anderson RH, Roux KJ (2016). BioID identification of lamin-associated proteins. Methods Enzymol 569, 3–22.

Mojica SA, Hovis KM, Frieman MB, Tran B, Hsia RC, Ravel J, Jenkins-Houk C, Wilson KL, Bavoil PM (2015). SINC, a type III secreted protein of Chlamydia psittaci, targets the inner nuclear membrane of infected cells and uninfected neighbors. Mol Biol Cell 26, 1918–1934.

Morriswood B, Havlicek K, Demmel L, Yavuz S, Sealey-Cardona M, Vidilaseris K, Anrather D, Kostan J, Djinovic-Carugo K, Roux KJ, *et al.* (2013). Novel bilobe components in Trypanosoma brucei identified using proximity-dependent biotinylation. Eukaryotic Cell 12, 356–367.

Mulholland CB, Smets M, Schmidtmann E, Leidescher S, Markaki Y, Hofweber M, Qin W, Manzo M, Kremmer E, Thanisch K, *et al.* (2015). A modular open platform for systematic functional studies under physiological conditions. Nucleic Acids Res 43, e112.

Nishimura T, Padamsi Z, Fakim H, Milette S, Dunham WH, Gingras AC, Fabian MR (2015). The eIF4E-binding protein 4E-T is a component of the mRNA decay machinery that bridges the 5′ and 3′ termini of target mRNAs. Cell Rep 11, 1425–1436.

Ritchie C, Cylinder I, Platt EJ, Barklis E (2015). Analysis of HIV-1 Gag protein interactions via biotin ligase tagging. J Virol 89, 3988–4001.

Rodriguez-Fraticelli AE, Bagwell J, Bosch-Fortea M, Boncompain G, Reglero-Real N, Garcia-Leon MJ, Andres G, Toribio ML, Alonso MA, Millan J, *et al.* (2015). Developmental regulation of apical endocytosis controls epithelial patterning in vertebrate tubular organs. Nat Cell Biol 17, 241–250.

Roux KJ, Kim DI, Burke B (2013). BioID: a screen for protein-protein interactions. Curr Protoc Protein Sci 74, Unit 19.23.

Roux KJ, Kim DI, Raida M, Burke B (2012). A promiscuous biotin ligase fusion protein identifies proximal and interacting proteins in mammalian cells. J Cell Biol 196, 801–810.

Savas JN, Toyama BH, Xu T, Yates JR 3rd, Hetzer MW (2012). Extremely long-lived nuclear pore proteins in the rat brain. Science 335, 942.

Schumacher MM, Elsabrouty R, Seemann J, Jo Y, DeBose-Boyd RA (2015). The prenyltransferase UBIAD1 is the target of geranylgeraniol in degradation of HMG CoA reductase. eLife 4, doi: 10.7554/eLife.05560.

Steed E, Elbediwy A, Vacca B, Dupasquier S, Hemkemeyer SA, Suddason T, Costa AC, Beaudry JB, Zihni C, Gallagher E, *et al.* (2014). MarvelD3 couples tight junctions to the MEKK1-JNK pathway to regulate cell behavior and survival. J Cell Biol 204, 821–838.

Tron CM, McNae IW, Nutley M, Clarke DJ, Cooper A, Walkinshaw MD, Baxter RL, Campopiano DJ (2009). Structural and functional studies of the biotin protein ligase from Aquifex aeolicus reveal a critical role for a conserved residue in target specificity. J Mol Biol 387, 129–146.

Ueda S, Blee AM, Macway KG, Renner DJ, Yamada S (2015). Force dependent biotinylation of myosin IIA by alpha-catenin tagged with a promiscuous biotin ligase. PLoS One 10, e0122886.

Ungricht R, Klann M, Horvath P, Kutay U (2015). Diffusion and retention are major determinants of protein targeting to the inner nuclear membrane. J Cell Biol 209, 687–703.

Van Itallie CM, Aponte A, Tietgens AJ, Gucek M, Fredriksson K, Anderson JM (2013). The N and C termini of ZO-1 are surrounded by distinct proteins and functional protein networks. J Biol Chem 288, 13775–13788.

Van Itallie CM, Tietgens AJ, Aponte A, Fredriksson K, Fanning AS, Gucek M, Anderson JM (2014). Biotin ligase tagging identifies proteins proximal to E-cadherin, including lipoma preferred partner, a regulator of epithelial cell-cell and cell-substrate adhesion. J Cell Sci 127, 885–895.

Vasu S, Shah S, Orjalo A, Park M, Fischer WH, Forbes DJ (2001). Novel vertebrate nucleoporins Nup133 and Nup160 play a role in mRNA export. J Cell Biol 155, 339–354.

Wilson KP, Shewchuk LM, Brennan RG, Otsuka AJ, Matthews BW (1992). Escherichia coli biotin holoenzyme synthetase/bio repressor crystal structure delineates the biotin- and DNA-binding domains. Proc Natl Acad Sci USA 89, 9257–9261.

Yeh C, Coyaud E, Bashkurov M, van der Lelij P, Cheung SW, Peters JM, Raught B, Pelletier L (2015). The deubiquitinase USP37 regulates chromosome cohesion and mitotic progression. Curr Biol 25, 2290–2299.

Zhou Z, Rawnsley DR, Goddard LM, Pan W, Cao XJ, Jakus Z, Zheng H, Yang J, Arthur JS, Whitehead KJ, *et al.* (2015). The cerebral cavernous malformation pathway controls cardiac development via regulation of endocardial MEKK3 signaling and KLF expression. Dev Cell 32, 168–180.

Zuccolo M, Alves A, Galy V, Bolhy S, Formstecher E, Racine V, Sibarita JB, Fukagawa T, Shiekhattar R, Yen T, *et al.* (2007). The human Nup107-160 nuclear pore subcomplex contributes to proper kinetochore functions. EMBO J 26, 1853–1864.